Single-Molecule Resolution of Protein Structure at Biomaterial Interfaces

Sean Yu McLoughlin[†], Mark Kastantin[†], Daniel K. Schwartz, and Joel L. Kaar[*]

Department of Chemical and Biological Engineering, University of Colorado, Boulder, CO 80309

[*]*Corresponding Author:*

Joel L. Kaar
University of Colorado Boulder
Department of Chemical and Biological Engineering
Campus Box 596
Boulder, CO 80309
Tel: (303) 492-6031
Fax: (303) 492-4341
Email: joel.kaar@colorado.edu

[†]S.Y.M. and M.K. contributed equally to this work.

SUPPLEMENTARY INFORMATION

Table of Contents

1) Supplementary Materials and Methods

1.1) OPH Labeling and Characterization

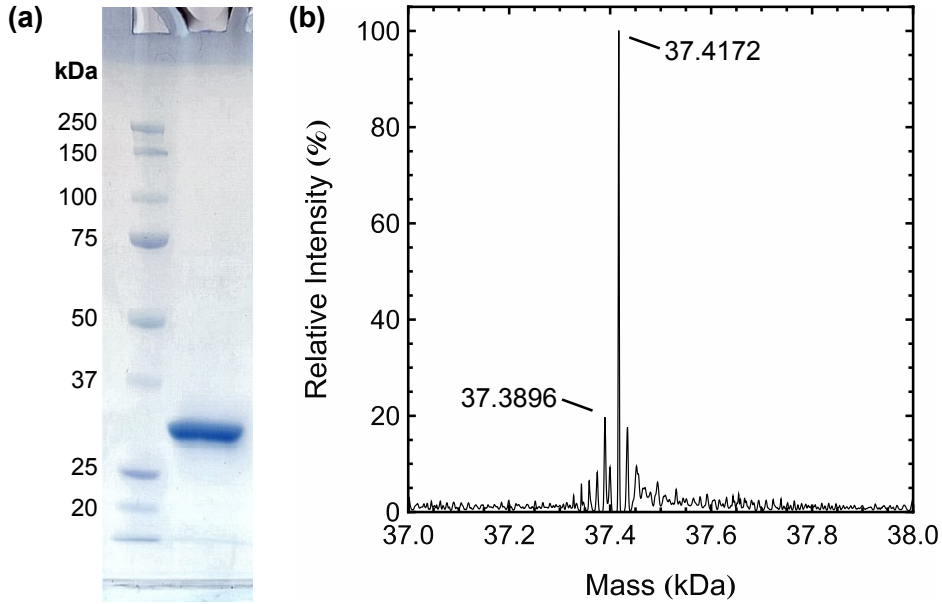

Figure S1. Characterization of OPH AzF175 by (a) SDS-PAGE, showing the purity of OPH AzF175, and (b) ESI mass spectrometry, confirming incorporation of AzF (the predicted mass for a single monomer of OPH AzF175 is 37,417 Da).

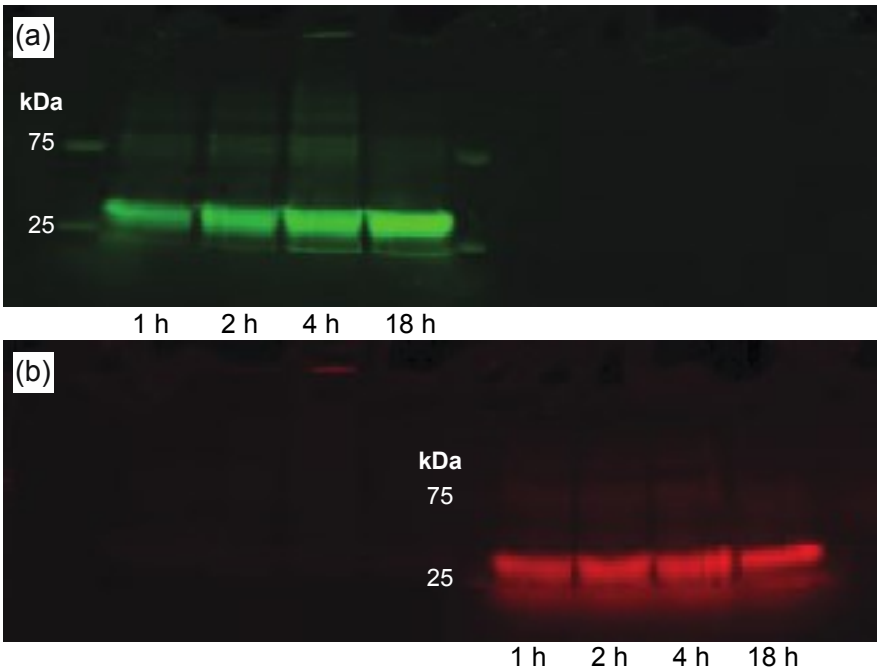

Figure S2. In-gel fluorescence imaging of single and dual-labeled OPH AzF175. The extent of single-labeling of OPH AzF175 with AF 555 and 647 was monitored as a function of labeling time. Direct excitation was performed on either AF 555 (a) or AF 647 (b). Molecular weight standards only fluoresce in the channel for AF 555.

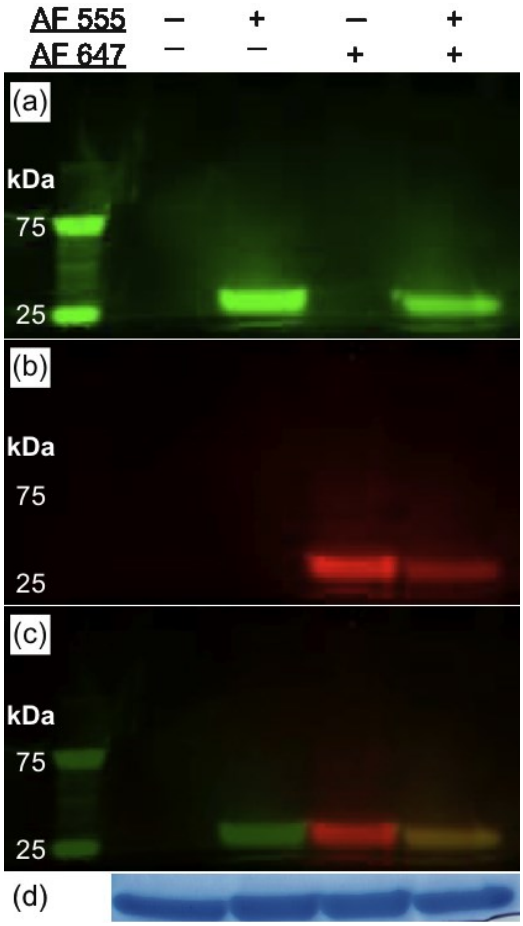

Figure S3. Dual-labeling of OPH AzF175 was confirmed by detection of AF 555 and 647 upon reaction of the enzyme with both fluorophores. The fluorophores used to label each enzyme are indicated above each gel lane. Direct excitation was performed on either AF 555 (a) or AF 647 (b), with an overlay of the two channels shown in (c). Molecular weight standards only fluoresce in the channel for AF 555. (d) Coomassie staining is shown as a control to confirm the presence of nearly equal concentrations of OPH AzF175 in all four lanes.

1.2) Measurement of OPH Activity

The activity of wild-type OPH and OPH AzF175 was assayed by measuring the rate of OPH-catalyzed hydrolysis of methyl parathion in buffer (100 mM sodium carbonate, 0.1 mM $CoCl_2$, pH 10.0) containing 0.1 mg/ml BSA at room temperature. Briefly, conversion of methyl parathion was measured by monitoring the release of the hydrolysis product *p*-nitrophenol by its absorbance at 405 nm. Kinetic parameters of the Michaelis-Mentin equation (V_{max} and K_M) were determined by non-linear least squares regression. These results, given in **Figure S4**, indicate that differences in the catalytic efficiency (k_{cat}/K_M) of wild-type OPH and OPH AzF175 were minimal. We therefore

conclude that replacement of lysine with AzF at position 175 did not drastically affect the activity and thus folding state of OPH.

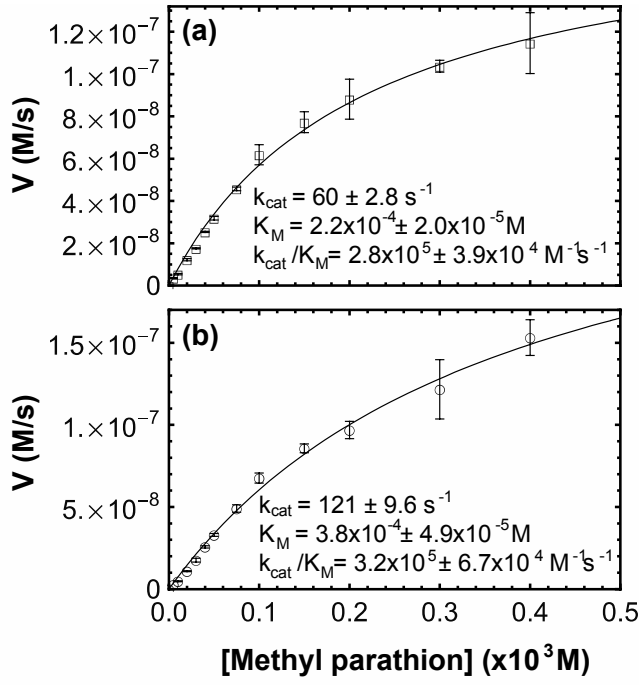

Figure S4. Impact of AzF incorporation on OPH activity. The kinetic constants (k_{cat} and K_M) were measured for (a) wild-type OPH and (b) OPH AzF175.

1.3) Surface and Solution Preparation for TIRFM Experiments

Initially, FS wafers (Mark Optics, Santa Ana, CA) were washed with Micro-90 cationic detergent (International Product Corp, Burlington, NJ) and thoroughly rinsed with water purified using reverse osmosis to 18 MΩ-cm. Wafers were subsequently immersed in warm piranha solution for 1 hour followed by thorough rinsing with purified water. OPH was introduced to FS wafers at a concentration of 5 x 10^{-9} M in buffer (20 mM glycine, 150 mM NaCl, 0.1 mM $CoCl_2$, pH 9.0). Additionally, unlabeled BSA (0.1 mg/ml final concentration) was added as a stabilizer since OPH in solution is unstable at the concentrations used for SM measurements. As a result of BSA addition at high concentrations, the dynamic interfacial behavior of dual-labeled OPH AzF175 described below was measured within a matrix of adsorbed BSA.

1.4) TIRFM Data Acquisition

SM-FRET TIRFM measurements were performed using a custom-built prism-based illumination system, flow cell maintained at 25.0 ± 0.1 °C, and Nikon TE-2000 microscope with 60x plan Apo water immersion objective and 1.5x post-objective magnification lens. Excitation was provided by a 532 nm, Cobolt (Solna, Sweden) Samba 50 mW diode-pumped solid-state laser that was coupled into a single mode fiber optic cable using a free space laser-fiber launch with a coupling efficiency of ~60 % (Oz Optics, Ottawa, Canada). Emitted light from the fiber optic was focused to a beam diameter at the sample (defined as the distance between the points in a Gaussian intensity profile at which the beam intensity is $1/e^2$ of its maximum value) of 48 μm.

To collect dual-channel images, an Optosplit II (Cairn Research, Kent, UK) image splitter with a T610LPXR dichroic mirror (Chroma, Bellows Falls, VT) with a nominal separation wavelength of 610 nm was used. Additional filters were used to further select for fluorescence emission in each channel. The donor channel used a FF01-585/40-25 bandpass filter (Semrock, Rochester, NY) centered at 585 nm with a 90 % transmission width of 40 nm. The acceptor channel used a FF01-685/40-25 bandpass filter (Semrock, Rochester, NY) centered at 685 nm with a 90 % transmission width of 40 nm. After fluorescence emission was split and filtered, each channel was projected onto a separate region of a Cascade-II: 512 EMCCD camera (Photometrics, Tucson, AZ) cooled to -70 °C. Sequential images were obtained at a frame rate of 10 s^{-1}. Channel alignment and object identification and tracking details were described previously (S1, S2) and our *Mathematica* code is provided as supplementary files.

The code contained in "SingleMoleculeTracking_FRET.nb" converts a movie of diffraction-limited fluorescent objects into a series of molecular trajectories. The data input is a series of TIFF images (contained in a single directory for each movie), where light from a donor channel has been projected onto the left hand side of the image and light from the acceptor channel has been projected onto the right hand side of the image. This code was written in *Mathematica* 8 and can run on versions

8 or 9. The associated library file, "ParticleTrackingFRET.m" is also required and the directory that contains this file must be specified in the code below (as noted by comments) based on the local directory structure. Comments are provided throughout the notebook using the notation "(*comment*)".

The tracking algorithm proceeds in 4 "Steps" that are further divided into sub-tasks contained in *Mathematica* evaluation cells. These steps and sub-tasks should be followed sequentially, from top to bottom, where each cell can be evaluated by clicking in the cell and using the "Enter" function on the keyboard, which is separate from the "Return" function (press shift-Enter or shift-Return on most keyboards). To open each Step and sub-task, double click on the bracket for the desired item on the right in the *Mathematica* environment, read the comments, change necessary parameters and file paths, and then evaluate the cells. Using the "Quit Kernel" function is recommended after each "Step" in order to clear memory of unnecessary information. Each "Step" begins by loading the relevant output of the previous "Step". It is also necessary to enable Dynamic Updating (often the default setting in *Mathematica*) in Step 1.

1.5) Calculation of the relative fluorophore-to-fluorophore distance

Following our previous treatment of SM-FRET data (S1), the absolute distance between fluorophores (r) was calculated from TIRFM data using the equation $r = \mu (F_D / F_A)^{1/6}$. Here, F_D and F_A are the intensities in the donor and acceptor channel, respectively, and the constant, μ, depends on the Förster radius (R_o) of the donor-acceptor pair as well as F_D and F_A measured at two known separations. Although it is straightforward to measure donor intensity in the absence of acceptor (i.e. $r \rightarrow \infty$), a second calibration intensity is difficult to measure due to difficulty in fixing fluorophore separation with sub-nanometer precision. Furthermore, when near a surface, R_o may also deviate from its expected value in bulk solution as a surface can potentially interact with the electronic structure of the dyes or can hinder rotation (S3). Due to these practical difficulties in determining μ and placing data

on an absolute distance scale, we chose to report our data using the relative fluorophore-to-fluorophore distance, $d = (F_D / F_A)^{1/6}$. Additionally, because donor-only labeled protein was undetectable in the acceptor channel, bleeding of donor into the acceptor channel was ignored in the calculation of d (see section 4). Acceptor-only labeled protein disappeared entirely upon excitation at 532 nm, indicating that direct excitation of the acceptor, which can affect d, was insignificant.

2) Raw Data

A sample movie of raw experimental data is provided as Supplementary Movie 1. This movie is 80 seconds long and plays in real time with an image acquisition time of 0.1 s. The width of each channel is 35 μm, the donor channel is on the left, and lighter pixels correspond linearly to greater intensity. Molecules frequently appear and disappear in each channel. The majority of molecules exhibit low mobility in the interfacial plane but the careful eye can identify some molecules that diffuse along the surface.

A second sample movie (Supplementary Movie 2) focuses on a few representative molecules that exhibit conformational changes. Three areas are circled and numbered such that one number indicates the same area in each channel. In each area, sequentially in time from 1 to 3, a molecule first appears in the acceptor channel. Acceptor intensity subsequently decreases significantly but increases concomitantly in the same area of the donor channel. This loss of FRET is consistent with a conformational change of OPH. This 38-second movie plays in real time with an image acquisition time of 0.1 s and the width of each channel is 35 μm.

Representative molecular trajectories are illustrated in **Figures S5** and **S6** by plotting fluorescence intensity in donor and acceptor channels, along with the corresponding *d*-values as a function of time. Information in these figures is displayed with a logarithmic time axis and *d*-values range from 0-2. A value of $d = 2$ is used for display purposes for all values $d \geq 2$ since negligible intensity in the acceptor channel yields anomalously large *d*-values. For display purposes, fluorescence intensity, in arbitrary units, is scaled by half of the maximum intensity in either channel during the given trajectory. Although this scale factor varied for each trajectory, it was within a factor of three over all trajectories; variation in absolute fluorescence intensity is discussed further in section 5.

Figure S5 shows trajectories that do not exhibit conformational changes while **Figure S6** shows trajectories that adsorb in one conformation and change conformations at one or more points before desorption. Each figure is further broken down by whether the molecule adsorbed in the folded

(a) or unfolded state (b). After separating trajectories based on these criteria, ten trajectories in each category were randomly chosen from subsets that exhibited surface residence times of at least 1 s. This criterion was chosen because the majority of trajectories were relatively short, and it is difficult to form a visual impression of data quality from these short trajectories.

Figure S6a shows ten trajectories that started folded and later unfolded, with anti-correlation between the intensity channels and a corresponding rise in *d*. Such anti-correlation is indicative of a change in FRET efficiency that can be caused by conformational change in OPH. This unfolding transition generally appeared to be irreversible, as high acceptor intensity was not observed after the initial transition. This phenomenon was also seen over the >30,000 trajectories used to construct **Figure 6**. Trajectories that were not believed to exhibit conformational changes, such as those in **Figure S5**, showed no intensity correlation between channels and occasionally exhibited positive intensity correlations due to statistical variation in the efficiency of donor excitation.

Figure S6b shows ten trajectories that started unfolded and later appeared to fold. Most often, trajectories in **Figure S6b** exhibited a brief drop in donor intensity without concomitant increase in acceptor intensity, meaning that the rise in *d*-value was not the result of a conformational change. This could explain why molecules that appeared to re-fold during their trajectory had surfaces residence times similar to molecules that were always denatured. **Figure S6b** also shows one trajectory that exhibited anti-correlation between intensity channels, indicating that the apparent re-folding event did correspond to the physical separation between donor and acceptor. However, based on the surface residence time data presented in **Figure 7**, we believe it is more likely that this apparent re-folding event led to a denatured OPH conformation with $d \leq 0.9$, rather than native OPH. We do not see any of these apparent re-folding events in **Figure S6a** because it seems that this low-*d* denatured conformation is relatively rare within the ensemble of denatured conformations.

The brief drops in donor intensity (and subsequent drop in *d*) in **Figure S6b** likely result from donor photoblinking for a fraction of the image acquisition that decreases the signal-to-noise ratio in

both channels and makes *d* temporarily an unreliable indicator of conformation. Brief drops in donor intensity are also observed in trajectories in **Figure S6a**, but it seems, by chance, that the noisy *d*-value remained high, rather than fell, in these few trajectories. It is likely that these anomalous apparent re-folding events are more likely to appear in **Figure S6b** than in **Figure S6a** by virtue of selection in the former for trajectories with at least one apparent re-folding event.

The opposite phenomenon, brief drops in acceptor intensity followed by a prolonged return to high intensity, was almost never observed. Such behavior would result in apparent unfolding followed by a prolonged return to a folded state; **Figure 6** indicates that this was rare. Signal in the acceptor channel may be more stable due to differences between donor and acceptor fluorophores, whereby the latter may be less likely to undergo photoblinking or may remain in the "off" state for shorter periods of time. It is also possible that objects that fluoresce primarily in the donor channel are more difficult to track and properly quantify their intensity. This could be a consequence of higher surface density of molecules appearing in this channel. Higher surface density of molecules could interfere with the intensity calculation if one molecule appears within the area used to calculate the local background for subtraction from the integrated intensity of another molecule. In our tracking algorithm, intensity is calculated as the sum of the values of the contiguous pixels identified as a single object minus a local background. The local background is calculated from the mean value of all pixels that are within two pixels of any that are identified as the object, but are not part of the object itself. Thus, multiple objects in close proximity could be identified as separate objects but raise the perceived local background and lower the calculated intensity of each.

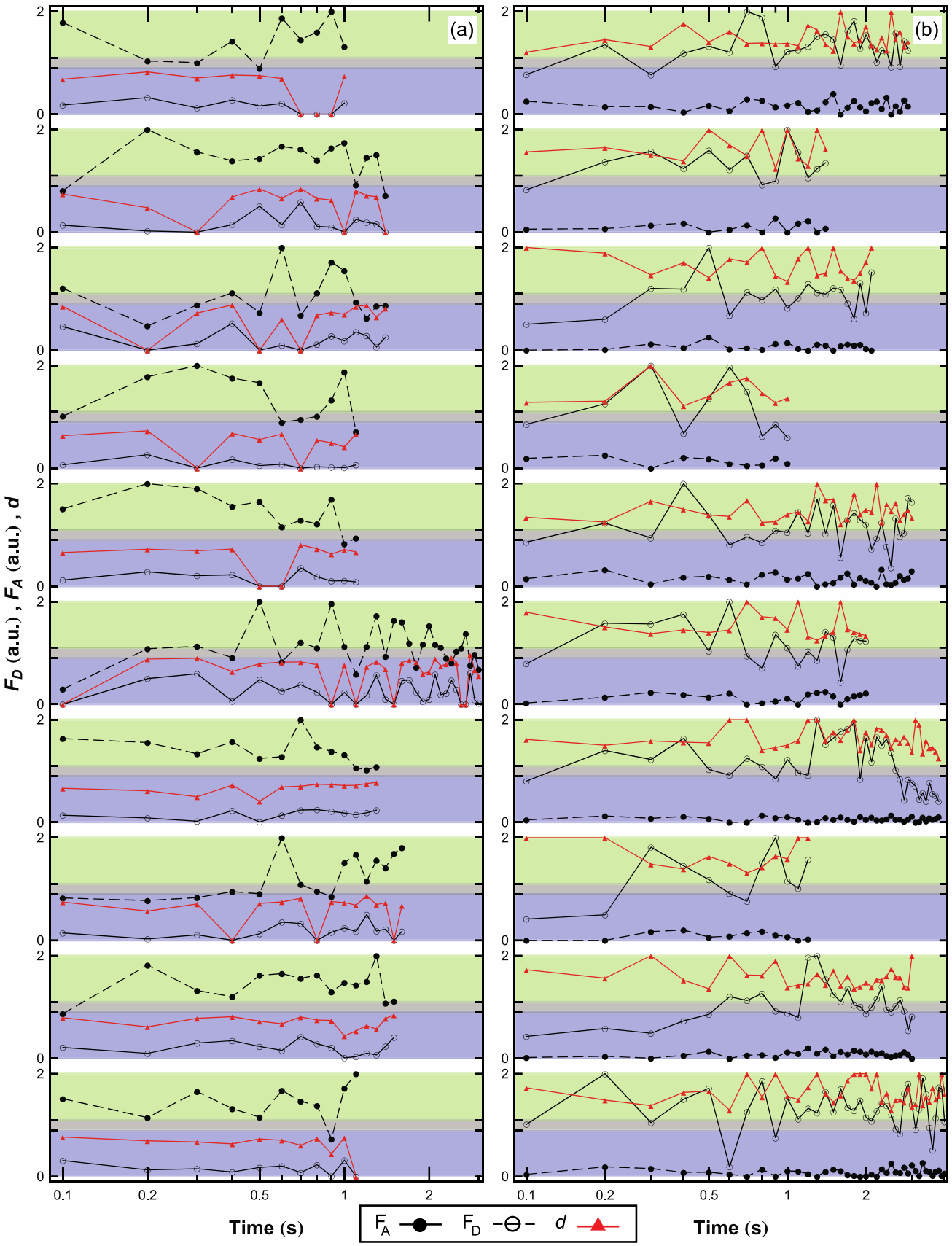

Figure S5. Sample trajectories show fluorescence in the acceptor channel (F_A), donor channel (F_D), and the corresponding d-values for proteins that are (a) always folded or (b) always unfolded.

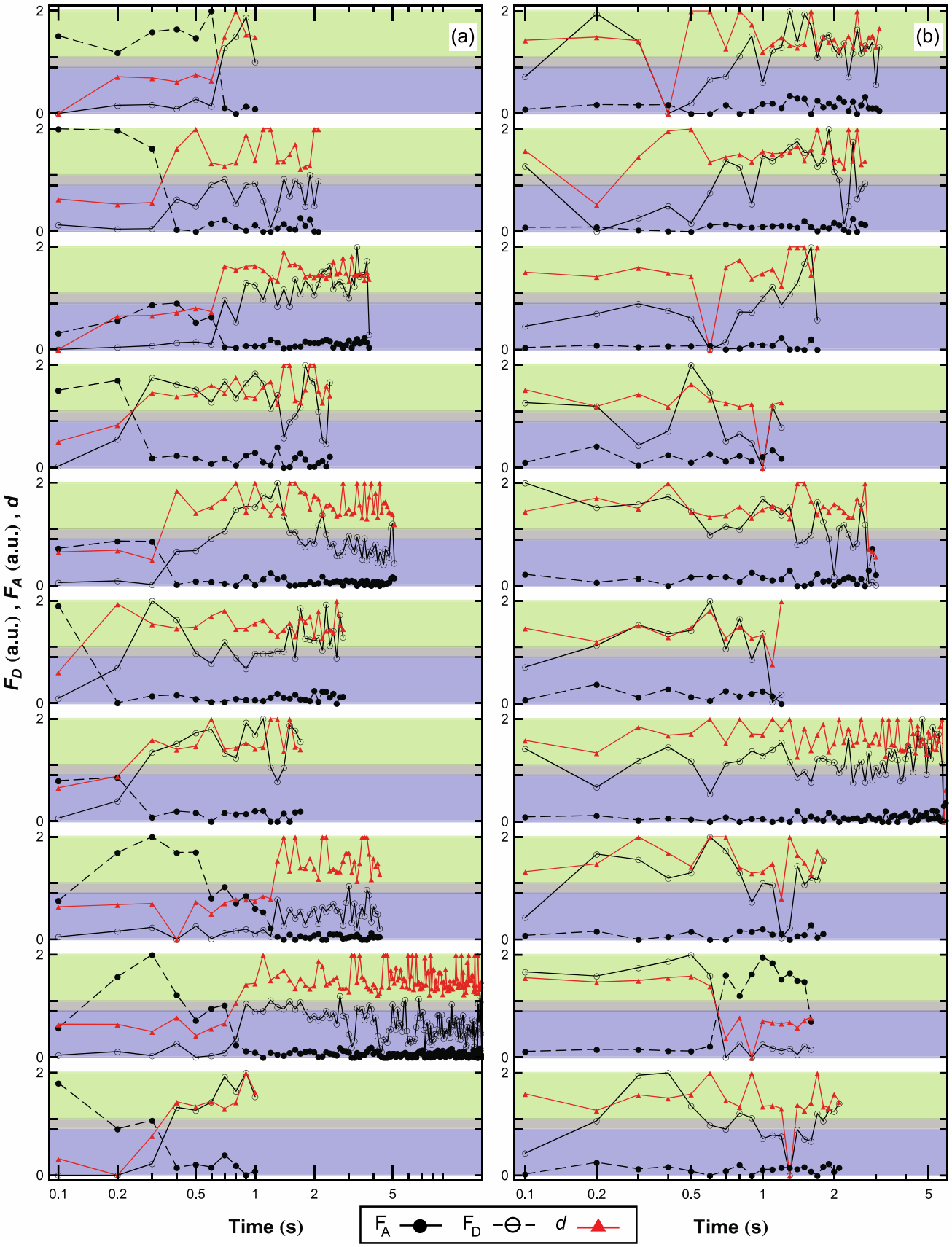

Figure S6. Sample trajectories show fluorescence in the acceptor channel (F_A), donor channel (F_D), and the corresponding d-values for proteins that are (a) initially folded or (b) initially unfolded.

3) Ensemble Measurements of OPH Conformation

The apparent, ensemble-averaged kinetics of surface-induced OPH unfolding were measured using a TIRF accessory and temperature controlled flow cell (TIRF Labs) for a fluorometer (Horiba, Fluoromax-4). A FS slide was maintained at 25.0 ± 0.1 °C and OPH was introduced in the same buffer that was used for single-molecule experiments but with an OPH concentration of 1 x 10^{-8} M. The average *d*-value was determined as a function of time by comparing the peak OPH fluorescence intensity at 568 nm (F_D) to that at 670 nm (F_A) using 555 nm excitation. The average *d*-value was found to increase exponentially over time (**Fig. S7**) and was fit to equation S1 where *t* is time, τ is the first-order time constant for unfolding, d_o is the initial *d*-value, and *A* is a constant equal to $(d_\infty - d_o)/ d_o$. Nonlinear least squares regression determined τ = (3.30 ± 0.01) x 10^4 s, and d_∞ = 1.31 ± 0.01 while d_o = 1.11 was determined experimentally. The unfolding time constant measured here is many orders of magnitude larger than in the single-molecule measurement, indicating that dynamic processes other than surface-induce unfolding dominate the apparent behavior of the ensemble.

$$\text{(S1)} \quad \frac{d}{d_o} = A\left(1 - e^{-t/\tau}\right) + 1$$

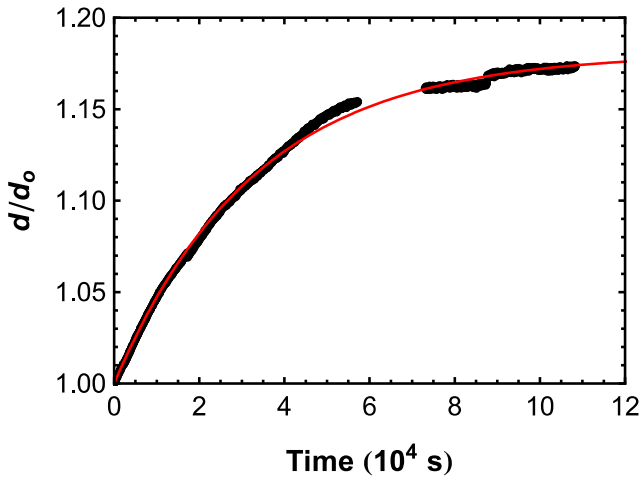

Figure S7. Kinetics of apparent OPH ensemble unfolding. The average *d*-value increases (FRET efficiency decreases) over time. The red line represents a fit to experimental data using equation S1.

In order to demonstrate the benefit of single-molecule measurements in determining OPH conformation, an average FRET measurement was made in bulk solution using a fluorometer (FP112, Slm Aminco, SLM Instruments). Samples were prepared by incubating 150 µl of protein with 0-3 M guanidine hydrochloride in 300 µl mixes for 30 min before transferring the mix to a 5 mm pathlength quartz microcuvette (Starna). The average *d*-value in solution was calculated, at varying concentrations of guanidine hydrochloride (Gdn), by measuring the ratio of peak OPH fluorescence intensity at 568 nm to that at 670 nm using 555 nm excitation. Although significant protein unfolding was expected when the Gdn concentration was increased from 0 to 3 M, the average *d*-value varied only slightly over this range (**Fig. S8**). A smaller dynamic range of relative *d*-values in ensemble measurements is likely due to inclusion of molecules that are mislabeled with two donors, whose fluorescence cannot be ignored. Donor-only labeled protein raises F_D but acceptor-only proteins contribute little to F_A due to minimal direct excitation of acceptors at 555 nm. Thus, an OPH population in the native state (i.e. when [Gdn] = 0) appears to have an anomalously high average *d*-value while the single-molecule measurement can select for proteins that are properly labeled. Differences between the values of d_∞ and d_o in the kinetic experiment and the *d*-values shown in **Fig. S8** for low and high [Gdn] are likely due to different labeling efficiencies between different batches of OPH.

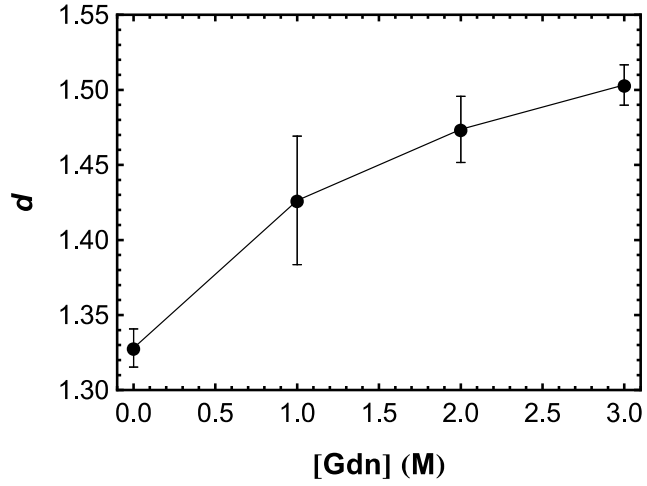

Figure S8. Relative fluorophore-to-fluorophore distance of fluorophores in dual-labeled OPH AzF175 in ensemble-averaged FRET measurements in solution.

4) Photobleaching and Photoblinking

Calculation of $d = (F_D / F_A)^{1/6}$ requires a measurement of fluorescence intensity in both the donor (F_D) and acceptor (F_A) channels. Both of these values are potentially susceptible to photophysical artifacts such as blinking, bleaching, direct excitation of acceptors, and cross-talk between channels. Similar issues are encountered in many other experiments that measure single-molecule fluorescence and we provide references to the interested reader as a starting point for how to treat such artifacts (S3-S7). In the present work, we assigned native and denatured conformation states of OPH to discrete, empirically derived ranges of d values. Consequently, we consider photophysical artifacts in the context of their ability to cause misidentifications of OPH conformation rather than seeking quantitative corrections of d.

4.1) Donor Photobleaching and Photoblinking

We found that direct excitation of the acceptor by the donor excitation source was negligible by labeling OPH exclusively with AF 647 (acceptor-only). As seen in **Figure S9a**, acceptor-only proteins could not be detected using a 532 nm excitation source. However, acceptor-only OPH was present on the surface, as seen in **Figure S9b**, where the excitation source was switched to a 642 nm laser (CrystaLaser, DL640-100). This result is expected given the large separation between the 532 nm donor excitation wavelength and the preferred excitation wavelengths for AF 647.

The practical consequence of this result is that photophysical effects that turn off donor fluorescence will also result in negligible fluorescence from the acceptor. For example, photobleaching of the donor species will cause apparent desorption of OPH. If the protein had not yet unfolded, our data filters would cause this trajectory to be ignored. If the protein had unfolded prior to donor photobleaching, the correct folded-state residence time would be measured. Consequently, donor photobleaching would have no effect on our measurement of unfolding kinetics.

Donor blinking that persists for short times (relative to the frame acquisition time of 100 ms) would reduce both F_D and F_A in proportion to the duration of the blinking event, lowering signal to noise. However, the value of d would not be affected to first order. Donor blinking that persists longer than the frame acquisition time would cause apparent desorption and then re-adsorption in a subsequent frame. Given typical time scales for blinking, which are on the order of a few tens of milliseconds (S4), this is not expected to be a common event. Furthermore, if OPH unfolded prior to the long-lived blinking event, it would have had no effect on the measurement of folded-state residence time and the molecule would reappear in the denatured state, causing this "broken trajectory" to be excluded from our analysis.

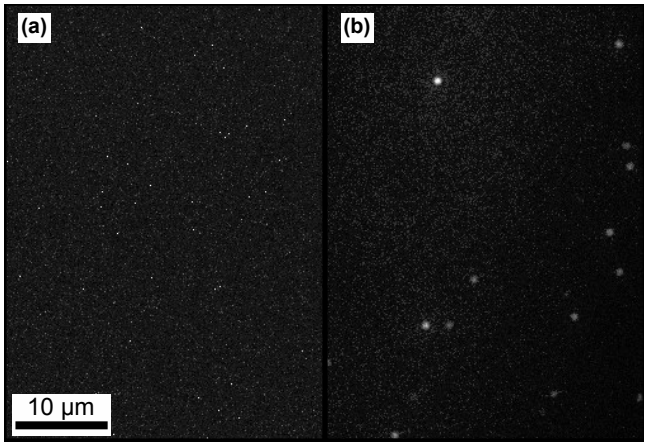

Figure S9. To indicate that direct excitation of acceptors is insignificant, OPH AzF175 was labeled only with acceptors. (a) With 532 nm excitation, no fluorophores were visible in the acceptor channel. (b) Acceptor-labeled proteins were clearly visible in the acceptor channel when 642 nm excitation was used.

Long-lived donor blinking would introduce artifacts in the data only if OPH unfolded after the blinking event. In this case, the first part of the broken trajectory would be ignored because no unfolding event was observed. The second part of the broken trajectory would be included in our analysis with an anomalously short folded-state residence time. Such an anomaly can generally be minimized by using a tracking algorithm that searches forward in time through multiple frames to look for an adsorption event in a location very close to the desorption location, thus bridging the blinking

event (S8). In the present work, we tested for possible long-lived donor photoblinking by searching for desorption events of folded OPH within a radius of 720 nm and within 500 ms prior to adsorption of initially-folded OPH that was later observed to unfold. Using this strategy, we found that a negligible fraction (less than 0.3%) of trajectories included in the analysis of unfolding kinetics were potentially affected by long-lived donor photoblinking.

4.2) Acceptor Photobleaching and Photoblinking

We found that donor fluorescence bleeding into the acceptor channel was negligible by labeling OPH exclusively with AF 555 (donor-only). Evidence for this assertion is that, when excited with a 532 nm laser, the tracking algorithm used could easily identify donor-only OPH in the donor channel, but not in the acceptor channel (**Fig. S10**). This result is expected given the large separation between the emission spectra of donor and acceptor fluorophores. We also considered acceptor fluorescence bleeding into the donor channel, although we did not detect acceptor-only OPH in the donor channel when using 532 nm excitation.

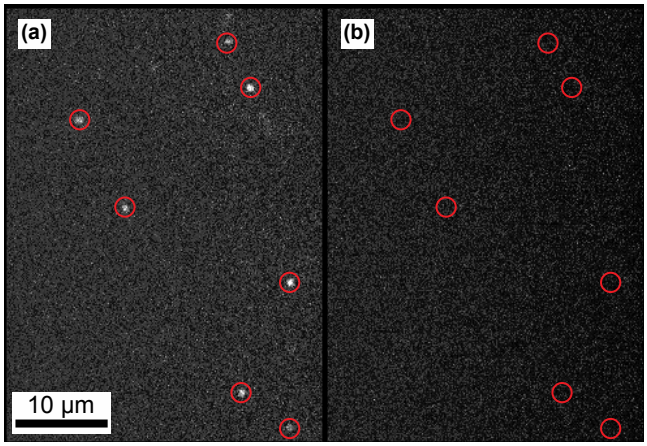

Figure S10. To indicate that bleeding of donor fluorescence into the acceptor channel is insignificant, OPH AzF175 was labeled only with donors. Individual proteins observed in (a) the donor channel were not observed in (b) the acceptor channel. Circles identify identical surface regions in the two channels.

An important consequence of negligible donor bleeding into the acceptor channel is that acceptor photobleaching would lead to a *d* value that permanently tends to infinity and to the anomalous perception that OPH had unfolded. However, as mentioned previously, **Figures 3a** and **4** show that the post-unfolding *d* value exhibits only modest fluctuations about a finite value of 1.4, indicating that measurable fluorescence intensity was observed in the acceptor channel and, in turn, that photobleaching was not apparent. Although trajectories occasionally exhibited negligible signal in the donor channel (noted by $d = 2$ in **Fig. 3a** and by the binned regions in **Fig. 2** and **Fig. 4**), we often observed that trajectories quickly reverted to lower, finite *d* values that indicated a fully functioning acceptor. Thus, our observations indicate that acceptor photobleaching did not significantly affect measurements of OPH unfolding kinetics.

Acceptor blinking on any time scale would result in an anomalously high *d* value and potentially shorten the apparent folded-state residence time. Such an artifact would result in random spikes in the value of *d* followed by a return to a *d*-value representative of the native state. Thus, blinking could result in a molecule that appears to randomly fold and unfold multiple times during its surface residence time. **Figure 4** shows that this behavior is only rarely observed, and that any fluctuations in *d* after the first unfolding observation are limited to short times after this initial event.

4.3) Effects of Photobleaching and Photoblinking on Apparent Desorption Events

An important conclusion of this work is that both native and unfolded OPH desorbs from dynamically. Given the above discussion of photobleaching and photoblinking effects, one might question whether these photophysical artifacts are responsible for the observed desorption events. Photoblinking would cause a molecule to disappear temporarily and reappear at some later time in a location near where it disappeared. We accounted for this effect when assessing OPH desorption by searching a radius of 720 nm for an adsorption event within 500 ms after each desorption event, regardless of OPH conformation. Using this strategy, approximately 10% of desorption events were

marked as possible anomalies due to photoblinking. Thus, at least 90% of OPH apparent desorption events were real, and **Figure 2** shows that a large majority of OPH desorbed from the denatured state. The fraction of desorption events that might have been due to long-lived photoblinking was higher than was found for photoblinking effects on the initial-state residence time distribution in section 4.1. This occurred because the faster unfolding time scale for OPH relative to that for desorption made it much more likely that photoblinking would occur after OPH unfolding than after desorption. To see the difference in time scales unfolding relative to desorption, compare **Figure 3b** to the "initially folded" dataset in **Figure 5**.

Donor photobleaching would cause a molecule to permanently disappear, and this would be indistinguishable from desorption for any one molecule. In this work we directly measured the first order time constant for donor photobleaching by immobilizing OPH on the surface and observing the apparent surface residence time distribution. Following piranha cleaning as described above, dry FS wafers underwent UV-ozone treatment for 1 h. Subsequently, we deposited a monolayer of 3-glycidoxypropyltirmethoxysilane (GPTMS) by exposing wafers to the vapors of a solution of toluene (85%), GPTMS (10%), and *n*-butylamine (5%) for 24 h at room temperature. The epoxide ring on GPTMS was used to react with primary amines on lysine residues of OPH in order to immobilize the protein. The GPTMS monolayer was exposed to an OPH solution at the same concentration and buffer composition used for single-molecule experiments in order to achieve single-molecule surface coverage of immobilized OPH. After 24 h, OPH solution was removed and the wafer was cleaned with a series of vigorous solvent rinses using water, ethanol, acetone, and toluene.

The OPH-immobilized wafers were then exposed to the same nominal buffer and laser power as was used elsewhere in this work. Under constant laser illumination, a time-lapse series was acquired, with 1 s between images. Imaging was performed in only one channel that accumulated fluorescence from both donor and acceptor fluorophores. Because we have previously shown that direct excitation of the acceptor is negligible, the presence of a molecule in this combined channel indicates that donor

photobleaching has not yet occurred. The length of time that each molecule remained on the surface was measured and used to construct an apparent surface residence time distribution. For protein that cannot desorb, this apparent surface distribution is a direct measure of photobleaching, which causes apparent desorption. As shown in **Figure S11**, the apparent surface residence time distribution exhibited a monoexponential decay with a characteristic time constant of 170 ± 10 s. **Figure S11** represents data combined from 4 separate experiments and the reported error represents the standard deviation when each of these experiments was analyzed separately. This time constant of 170 s is roughly two orders of magnitude longer than time scales relevant for desorption or unfolding found in this work. Thus, we believe photobleaching has a negligible effect on the results presented here.

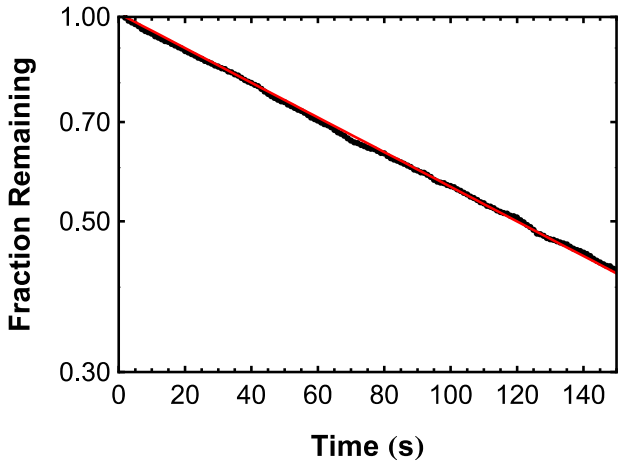

Figure S11. Apparent surface residence time distribution of immobilized OPH. Molecules are covalently attached to the surface and so apparent desorption is a result of photobleaching. Combined results from 4 experiments indicate a monoexponentially decaying distribution with a first order time constant of 170 ± 10 s.

5) Evidence Against the Presence of OPH Aggregates

As mentioned previously, OPH exists in its native state as a homodimer. Although unlikely, we also considered the possibility of higher aggregates as these species would change the interpretation of FRET data presented in this work. As clarification, the term "aggregates" will hereafter refer to clusters of dimeric OPH (leading to tetramers, hexamers, etc.). Although many proteins appear in our movies, sometimes close together, single-molecule tracking requires that the surface density of proteins is extremely low, and that molecules diffuse slowly relative to the average separation between them. Thus it is unlikely that aggregation events occur by diffusion of OPH in the interfacial plane. More specifically, the point spread function of fluorescence from a single protein in our optical system is a two-dimensional Gaussian that typically registers in a square array of pixels between 3 and 4 pixels on a side. Thus, proteins must be separated by at least 5 pixels (corresponding to ~0.7 μm, roughly 100x larger than the size of the OPH dimer) in order to appear as separate, diffraction-limited objects. Movies displayed in section 2 confirm that individual spots are resolvable for the vast majority of trajectories.

It is also possible that OPH aggregates are present in solution and adsorb onto the surface in an aggregated state. In this case, we would identify all proteins as a single object with a total fluorescence intensity that scales with the number of OPH dimers in the cluster. Our data allows us to test for this phenomenon explicitly by observing the summed intensity in both the donor and acceptor channels. Rather than quantifying aggregation using the intensity in any one channel, the summed intensity is preferred because this value is proportional to the total number of fluorophores on the object rather than the efficiency of FRET, which depends on conformation.

The median value of the summed intensity was recorded for each trajectory and assembled into a probability histogram as shown in **Figure S12**, which is normalized so that the most probable median intensity was 1 arbitrary unit. We observed a continuous distribution with the vast majority of observations occurring between 0 and 3 units. Importantly, we found a single peak in this distribution

rather than multiple peaks at integer multiples of the intensity of an OPH dimer. We have previously identified a correspondence between aggregation and a multi-modal distribution of fluorescence intensities in other systems (S9), but this is not the case here. The observed variation in the distribution of median summed intensities is likely due to statistical fluctuations in the number of successful fluorescence events of a given fluorophore combined with some variation in identifying and quantifying this fluorescence using our automated tracking algorithm. Furthermore, the non-uniform, Gaussian beam profile of our focused laser excitation source allows excitation power to vary by as much as a factor of 2.5 throughout our field of view, further increasing the spread of measured intensities. In conclusion, these data indicate that OPH aggregates do not contribute significantly to the data presented in this work.

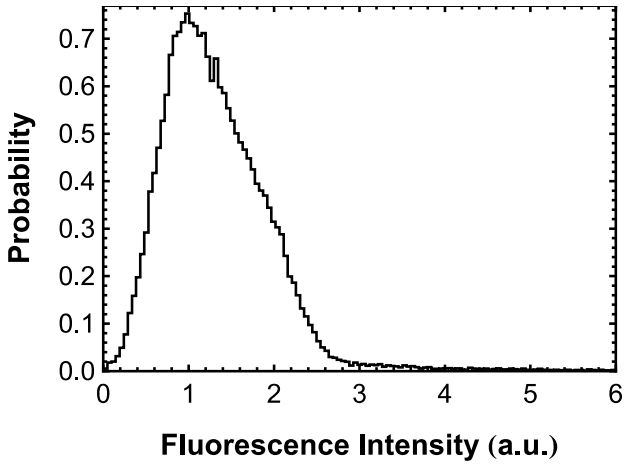

Figure S12. Probability distribution of median fluorescence intensity summed over the donor and acceptor channels. The most probably intensity value was set to one unit.

SUPPLEMENTARY REFERENCES

S1. Kastantin M & Schwartz DK (2011) Connecting rare DNA conformations and surface dynamics using single-molecule resonance energy transfer. *ACS Nano* 5(12):9861-9869.

S2. Kastantin M, Walder R, & Schwartz DK (2012) Identifying mechanisms of interfacial dynamics using single-molecule tracking. *Langmuir* 28(34):12443-12456.

S3. Lakowicz JR (2006) *Principles of fluorescence spectroscopy* (Springer, Singapore) 3rd Ed pp xxvi, 954.

S4. Vogelsang J*, et al.* (2008) A reducing and oxidizing system minimizes photobleaching and blinking of fluorescent dyes. *Angew. Chem., Int. Ed.* 47(29):5465-5469.

S5. Patra D (2008) Application and new developments in fluorescence spectroscopic techniques in studying individual molecules. *Appl. Spectrosc. Rev.* 43(5):389-415.

S6. Rasnik I, McKinney SA, & Ha T (2006) Nonblinking and longlasting single-molecule fluorescence imaging. *Nat. Methods* 3(11):891-893.

S7. Ruttinger S*, et al.* (2006) Accurate single-pair Forster resonant energy transfer through combination of pulsed interleaved excitation, time correlated single-photon counting, and fluorescence correlation spectroscopy. *J. Biomed. Opt.* 11(2):024012.

S8. Claytor K*, et al.* (2009) Accurately determining single molecule trajectories of molecular motion on surfaces. *J. Chem. Phys.* 130(16):164710.

S9. Kastantin M, *et al*. (2011) Single-molecule resolution of interfacial fibrinogen behavior: Effects of oligomer populations and surface chemistry. *J. Am. Chem. Soc.* 133(13):4975-4983.